Establishment of Immunodeficient Retinal Degeneration Model Mice and Functional Maturation of Human ESC-Derived Retinal Sheets after Transplantation

AUTHOR(S):

Iraha, Satoshi; Tu, Hung-Ya; Yamasaki, Suguru; Kagawa, Takahiro; Goto, Motohito; Takahashi, Riichi; Watanabe, Takehito; ... Tanihara, Hidenobu; Takahashi, Masayo; Mandai, Michiko

CITATION:

Iraha, Satoshi ...[et al]. Establishment of Immunodeficient Retinal Degeneration Model Mice and Functional Maturation of Human ESC-Derived Retinal Sheets after Transplantation. Stem Cell Reports 2018, 10: 1059-1074

ISSUE DATE:

2018-03-13

URL:

http://hdl.handle.net/2433/230369

Stem Cell Reports
Article
ISSCR
OPEN ACCESS

Establishment of Immunodeficient Retinal Degeneration Model Mice and Functional Maturation of Human ESC-Derived Retinal Sheets after Transplantation

Satoshi Iraha,[1,2,3,10] Hung-Ya Tu,[1,10] Suguru Yamasaki,[1,4] Takahiro Kagawa,[5] Motohito Goto,[5] Riichi Takahashi,[5] Takehito Watanabe,[1] Sunao Sugita,[1] Shigenobu Yonemura,[6,7] Genshiro A. Sunagawa,[1] Take Matsuyama,[1] Momo Fujii,[1] Atsushi Kuwahara,[4] Akiyoshi Kishino,[4] Naoshi Koide,[1] Mototsugu Eiraku,[8] Hidenobu Tanihara,[2] Masayo Takahashi,[1,3] and Michiko Mandai[1,9,*]

[1]Laboratory for Retinal Regeneration, Center for Developmental Biology, RIKEN, Kobe, Hyogo 650-0047, Japan
[2]Department of Ophthalmology, Faculty of Life Sciences, Kumamoto University, Kumamoto 860-8556, Japan
[3]Application Biology and Regenerative Medicine, Graduate School of Medicine, Kyoto University, Kyoto 606-8501, Japan
[4]Regenerative and Cellular Medicine Office, Sumitomo Dainippon Pharma Co., Ltd., Kobe, Hyogo 650-0047, Japan
[5]Central Institute for Experimental Animals, Animal Resources and Technical Research Center, Kawasaki, Kanagawa 210-0821, Japan
[6]Ultrastructural Research Team, RIKEN Center for Life Science Technologies., Kobe, Hyogo 650-0047, Japan
[7]Department of Cell Biology, Tokushima University Graduate School of Medical Science, Tokushima 770-8503, Japan
[8]Laboratory for in vitro Histogenesis, RIKEN Center for Developmental Biology, Kobe, Hyogo 650-0047, Japan
[9]RIKEN Program for Drug Discovery and Medical Technology Platforms (DMP), Kobe, Hyogo 650-0047, Japan
[10]Co-first author
*Correspondence: mmandai@cdb.riken.jp
https://doi.org/10.1016/j.stemcr.2018.01.032

SUMMARY

Increasing demand for clinical retinal degeneration therapies featuring human ESC/iPSC-derived retinal tissue and cells warrants proof-of-concept studies. Here, we established two mouse models of end-stage retinal degeneration with immunodeficiency, NOG-*rd1-2J* and NOG-*rd10*, and characterized disease progress and immunodeficient status. We also transplanted human ESC-derived retinal sheets into NOG-*rd1-2J* and confirmed their long-term survival and maturation of the structured graft photoreceptor layer, without rejection or tumorigenesis. We recorded light responses from the host ganglion cells using a multi-electrode array system; this result was consistent with whole-mount immunostaining suggestive of host-graft synapse formation at the responding sites. This study demonstrates an application of our mouse models and provides a proof of concept for the clinical use of human ESC-derived retinal sheets.

INTRODUCTION

Cell transplantation therapies using embryonic stem cell (ESC) and induced pluripotent stem cell (iPSC)-derived retinal tissue (ESC/iPSC retina) or cells have emerged as therapeutic options for retinal degeneration following recent breakthroughs. A number of groups have shown that transplantation of postnatal or ESC/iPSC-derived photoreceptor precursor cells can integrate and restore visual function after transplantation into an adult mouse model of retinal degeneration that retains the photoreceptor layer (outer nuclear layer [ONL]) (Lamba et al., 2009; Pearson et al., 2012; Tucker et al., 2011), although the mechanism by which photoreceptor function is restored has recently been suggested as rescue of surviving host cells by material transfer from donor cells, rather than by direct cell integration (Pearson et al., 2016; Santos-Ferreira et al., 2016a; Singh et al., 2016). Another breakthrough was the introduction of a protocol for self-organizing three-dimensional retinal differentiation from mouse ESCs (mESCs) (Eiraku et al., 2011), which was successfully adapted to human ESCs (hESCs) (Nakano et al., 2012) and human iPSCs (hiPSCs) (Zhong et al., 2014). Since then, in addition to the increasing number of reports that mouse or hESC/iPSC-derived photoreceptor precursors could integrate into, or transfer materials to, host ONL (Decembrini et al., 2014; Gonzalez-Cordero et al., 2013; Hambright et al., 2012; Santos-Ferreira et al., 2016b; Zhu et al., 2017), we and others have reported that transplanted ESC/iPSC retinal sheets or photoreceptors can make *de novo* synaptic connections and restore some visual functions in end-stage retinal degeneration models with no ONL structure (Assawachananont et al., 2014; Barnea-Cramer et al., 2016; Mandai et al., 2017; Shirai et al., 2015).

Human ESCs take as long as 200 days to differentiate into fully mature retina, which was presented by immunohistology in monkeys and also by the presence of outer segments in nude rats following the transplantation (Shirai et al., 2015). However, hESC retinal cells do not always mature properly in xenograft rodent models, especially when there is damage due to the surgical procedure (Hambright et al., 2012). Although some researchers reported successful transplantation of human cells in rodent hosts with immunosuppression, graft survival was usually monitored for a relatively short period such as within several weeks (Barnea-Cramer et al., 2016). Even with

immunosuppression, mild rejection can be observed that may inhibit synaptic formation (Larsson et al., 2000). For these reasons, SD-Foxn1 Tg(S334ter)3LavRrrc rats were developed (Seiler et al., 2014, 2017), and we reported that transplanted hESC retina developed an organized ONL with potential synaptic connections to host bipolar cells (Shirai et al., 2015). Although the SD-Foxn1 Tg(S334ter) 3LavRrrc rat is a good model for proof-of-concept studies using human cells, mouse models for which abundant phenotypic studies and gene expression databases are available would be more desirable. Moreover, mice are more accessible to genetic manipulations such as introduction of reporter genes. Recently, Zhu et al. (2017) reported up to 9 months' survival of transplanted hESC-derived photoreceptors with some function in IL2Rg-deficient CRX-mutant mice, but the possibility of material transfer cannot be excluded due to the remaining host photoreceptors. Thus, immunodeficient end-stage retinal degeneration mouse models with absent ONL structure would be useful for preclinical studies featuring transplantation of hESC/iPSC-derived cells and tissues.

In 2002, Ito et al. (2002) established an appropriate animal recipient model for xenotransplantation: non-obese diabetes (NOD)/Shi-SCID, IL2Rg^{null} (NOG) mice. Characteristics of NOG mice are as follows: (1) lack of T, B, and natural killer (NK) cells; (2) reduced function of macrophage and dendritic cells; and (3) lack of complement activity. This NOG mouse model has been used to study the human lymphoid system by transplanting human cord blood-derived hematopoietic stem cells, and is very useful for testing the tumorigenicity of human cells (Kanemura et al., 2014; Machida et al., 2009; Watanabe et al., 2011).

In this report, we established mouse models suitable for human retinal cell transplantation by introducing phosphodiesterase 6B (*Pde6b*) mutant allele from retinal degeneration (rd) mouse models into NOG background. *Pde6b*$^{rd1/rd1}$ (*rd1*) and *Pde6b*$^{rd10/rd10}$ (*rd10*) mice are well-studied and frequently used animal models of retinal degeneration with different degeneration speeds. The missense point mutation in *Pde6b* carried in these mice is also found as a causal gene of human autosomal recessive retinitis pigmentosa (RP). *Rd1* presents a phenotype of progressive retinal degeneration similar to that seen in C3H and *Pde6b*$^{rd1\text{-}2J/rd1\text{-}2J}$ (*rd1-2J*) mice, with the onset of photoreceptor degeneration at around postnatal day 16 (P16), and loss of photoreceptors within the first 3–4 postnatal weeks (Chang et al., 2007; Kim et al., 2008). *Rd10* exhibits a slightly slower photoreceptor degeneration starting between P16 and P20, and most of the photoreceptors disappear by P60 (Pennesi et al., 2012).

We first characterized the degeneration phenotype in these rd mice with NOG background because immune responses have been suggested to accompany or modulate the pathogenesis of neurodegenerative diseases (Cuenca et al., 2014; González et al., 2014; Jin et al., 2016; Noailles et al., 2016; Yoshida et al., 2013a, 2013b; Zabel et al., 2016; Zeng et al., 2005; Zhao et al., 2015). *Rd1* mice in the background of SCID, or in combination with RAG-1 knockout (no functional B and T cells) or a C1qα knockout (no functional classical complement activation pathway) (Rohrer et al., 2007) or NOD (no functional B and T cells and low activity of NK cells) (Mishra et al., 2017) showed no difference in the degeneration speed, while *rd10* mice with *Ccr2* knockout (Guo et al., 2012) and *Cx3cr1* knockout (Peng et al., 2014) exhibited slower degeneration. We next transplanted hESC retinal sheets, to confirm the long-term survival and functional integration of graft cells in NOG-*rd1-2J* mice by immunohistochemistry and electrophysiology recording.

RESULTS

Development of NOG-*rd1-2J* and NOG-*rd10* Mice, Retinal Degeneration Models with Severe Immunodeficiency

We used marker-assisted breeding to develop immunodeficient retinal degeneration mouse models for transplantation of hESC retina (summarized in Figure 1A; details in Experimental Procedures). Using this marker-assisted breeding, we were able to obtain two types of NOG-rd transgenic mice within a relatively short period of 420 days.

Optical coherence tomography (OCT) examination revealed normal ONL thickness in NOG-*Pde6b*$^{rd/+}$ mice but loss of ONL in NOG-*Pde6b*$^{rd/rd}$ littermates at postnatal week 8 (Figures 1B and 1C). Electroretinograms (ERGs) showed detectable a and b waves in NOG-*Pde6b*$^{rd/+}$ mice; however, no ERG responses to 2.0 log cd/m^2/s stimulus were recorded in NOG-*Pde6b*$^{rd/rd}$ littermates (Figures 1D and 1E). At postnatal week 12, immunohistochemical analysis showed indistinguishable ONL thickness between NOG-*Pde6b*$^{+/+}$ and NOG-*Pde6b*$^{rd1\text{-}2J/+}$, or NOG-*Pde6b*$^{+/+}$ and NOG-*Pde6b*$^{rd10/+}$ littermates, whereas the ONL was substantially thinner in NOG-*Pde6b*$^{rd1\text{-}2J/rd1\text{-}2J}$ and NOG-*Pde6b*$^{rd10/rd10}$ mice with no immunoreactivity to rhodopsin (RHO) or cone opsins (OPN1MW and OPN1SW) (Figures 1F and 1G). These results indicate that photoreceptor degeneration occurred in both of our newly generated mouse models. We also checked the spleen cells in these four mouse lines (Figure S1). CD4$^+$ cells (helper T cells), CD8$^+$ cells (cytotoxic T cells), CD19$^+$ cells (B cells), and NKp46$^+$ cells (NK cells) showed markedly lower ratios in spleen cells from both NOG-*rd1-2J* mice and NOG-*rd10* mice compared with their counterparts from *rd1-2J* mice and *rd10* mice, confirming the immunodeficient state

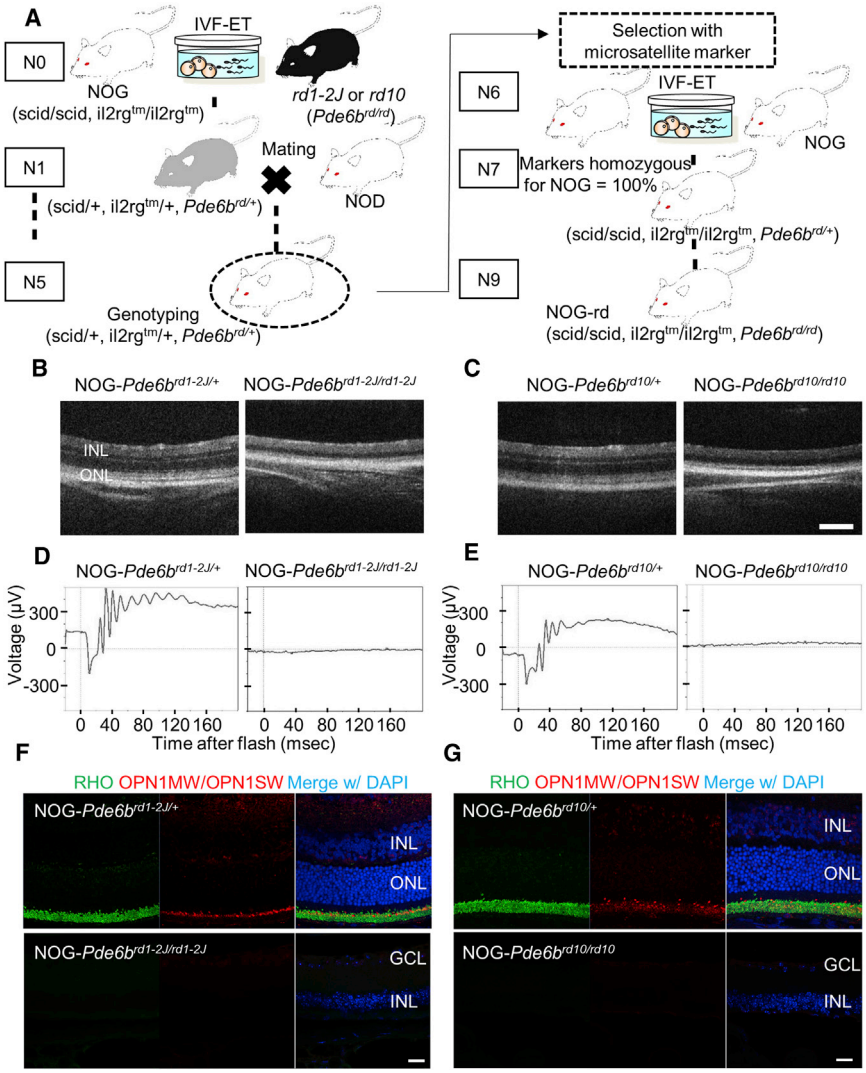

Figure 1. Breeding of NOG-*rd1-2J* Mice and NOG-*rd10* Mice, Immunodeficient and Retinal Degeneration Mouse Models

(A) Schema of the marker-assisted screening methods. The first generation (N1) was obtained by *in vitro* fertilization (IVF) of male rd mice and female NOD/Shi-scid, IL2Rg^{null} (NOG) mice. Next, female N1 mice were mated with male non-obese diabetes (NOD) mice until we obtained the N5. Marker-assisted selection with the microsatellite markers was then performed to select the mice closest to NOD strain. Finally, the selected male mice and NOG females were used for IVF to obtain the NOG line.

(B–G) Degeneration of photoreceptor cells were confirmed in NOG-*rd1-2J* mice and NOG-*rd10* mice (NOG-rd mice). OCT images of NOG-*Pde6b*$^{rd1-2J/+}$ and NOG-*Pde6b*$^{rd1-2J/rd1-2J}$ mice (B), NOG-*Pde6b*$^{rd10/+}$ and NOG-*Pde6b*$^{rd10/rd10}$ mice (C) at postnatal week 8. No outer nuclear layer was observed in NOG-*Pde6b*$^{rd1-2J/rd1-2J}$ and NOG-*Pde6b*$^{rd10/rd10}$ mice. ERG analysis of NOG-*Pde6b*$^{rd1-2J/+}$ and NOG-*Pde6b*$^{rd1-2J/rd1-2J}$ mice (D), NOG-*Pde6b*$^{rd10/+}$ and NOG-*Pde6b*$^{rd10/rd10}$ mice (E) were conducted at the age of 10 months. No ERG responses were detected with 2.0 log cd/m^2/s flash light in NOG-*Pde6b*$^{rd1-2J/rd1-2J}$ and NOG-*Pde6b*$^{rd10/rd10}$ mice. Immunohistochemical analyses of 12-week-old mice are shown in (F) and (G). In NOG-*Pde6b*$^{rd1-2J/rd1-2J}$ and NOG-*Pde6b*$^{rd10/rd10}$ mice, both RHO (rhodopsin) and OPN1MW/OPN1SW (cone opsins) were absent. Cone opsins were labeled with a mixture of anti-M/L and S opsin antibodies.

INL, inner nuclear layer; ONL, outer nuclear layer; GCL, ganglion cell layer. Scale bars, 200 μm (B and C) and 50 μm (F and G).

(e.g., lack of T cells, B cells, and NK cells) of these NOG-rd mice. Interestingly, we also found enlarged populations of CD11b$^+$ cells (including monocytes, macrophages, and microglia) in the spleens of both NOG mice, whereas the spleen cells of both *rd1-2J* and *rd10* mice had reduced populations of these CD11b$^+$ cells (Figure S1).

Earlier Degeneration Onset Observed in *rd10* Mice with NOG Background but Not in *rd1-2J* with NOG Background

We performed immunohistochemical analyses to compare degeneration time courses between *rd1-2J* and NOG-*rd1-2J* mice (Figure 2A), or *rd10* and NOG-*rd10* mice (Figure 2B). We evaluated the time courses of ONL loss using hierarchical Bayesian modeling (Figures S2A–S2C; see also Experimental Procedures and Data S1). The ONL thickness was not significantly different between *rd1-2J* and NOG-*rd1-2J* at P7, P14, and P21, with distributions of estimated ONL thickness nearly overlapping (Figures 2C and S2B; Table S2). Many Iba-1 (AIF1)-positive microglia infiltrated at P14 but mostly disappeared at P21 along with photoreceptor loss (Figure 2C), consistent with a previous report (Zhao et al., 2015). In contrast, the ONL of NOG-*rd10* mice was thinner than that of *rd10* mice at P16, P23, and P30, implying earlier degeneration in the NOG background with concomitant microglia infiltration (Figures 2B and 2C). The timing of photoreceptor apoptosis was next assessed in *rd10*; only a few TUNEL-positive apoptotic cells were found in the ONL, with microglia limited to the inner and outer plexiform layers (IPL/OPL) at P16 in *rd10* mice

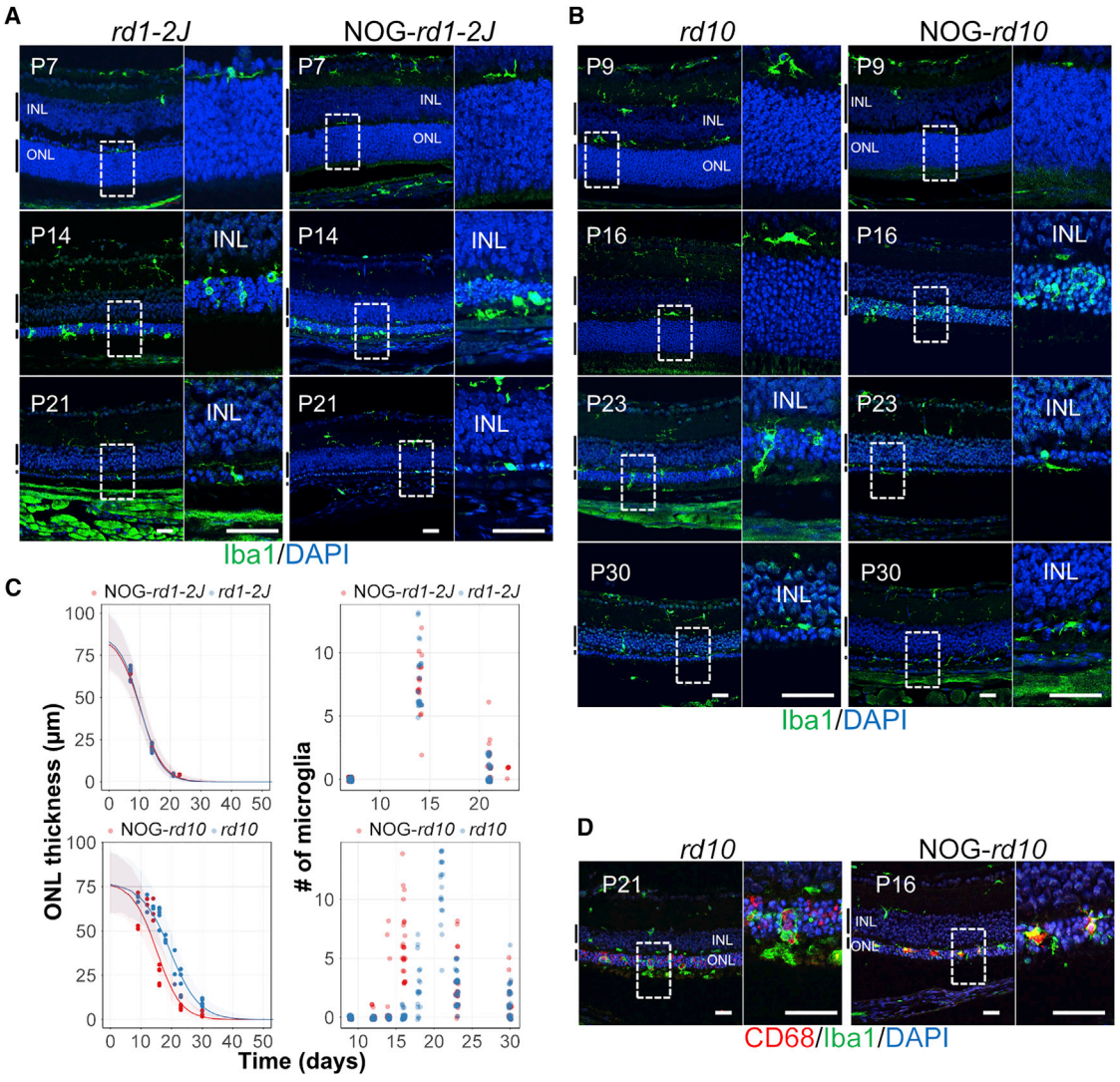

Figure 2. Degeneration Time Course in rd Mice and NOG-rd Mice

(A and B) Changes in ONL thickness and microglia infiltration in *rd1-2J* (A) and *rd10* (B) paired with their NOG counterparts, respectively, with AIF1 immunostaining (Iba-1 microglia marker, green).

(C) The retinal degeneration time courses were indicated by the ONL thickness in all four mouse lines (n = 2–5 for each time point in each line). *Rd1-2J* and *rd10* were marked as red dots, with their NOG counterparts in blue. Lines and shaded areas, respectively, denote the median and the 95% credible interval of the estimated distribution of the thickness. Note that the estimated distributions of both *rd1-2J* strains are mostly overlapped, while the NOG-*rd10* mice showed earlier degeneration than *rd10* mice (n = 2–5). These analysis details are available in Supplemental Experimental Procedures, Figure S2, and Data S1. Numbers of microglia found in the ONL at different time points indicates NOG-*rd10* mice tended to exhibit earlier microglia infiltration into the ONL than *rd10* mice.

(D) Pro-inflammatory characteristic of infiltrating microglia (AIF1, green) in *rd10* and NOG-*rd10* mouse retinas was shown by staining against CD68 (active microglia marker, red).

INL, inner nuclear layer; ONL, outer nuclear layer; these layers are also indicated by the side bars. Scale bars, 30 μm.

and P12 in NOG-*rd10* mice, followed by the dramatic increase of TUNEL-positive cells in the ONL at P18 in *rd10* mice and P14 in NOG-*rd10* mice (Figure S3A). The ONL thickness was reduced to less than half at P21 in *rd10* mice and at P16 in NOG-*rd10* mice (Figure S3A). This observation was consistent with the estimation that the half-life period of the ONL degeneration is shorter in NOG-*rd10* mice than in *rd10* mice (95% credible interval for the half-life period was 2.61–5.87 days; mean 4.28 days) (Figures 2C and S2C; Table S2). Microglia were

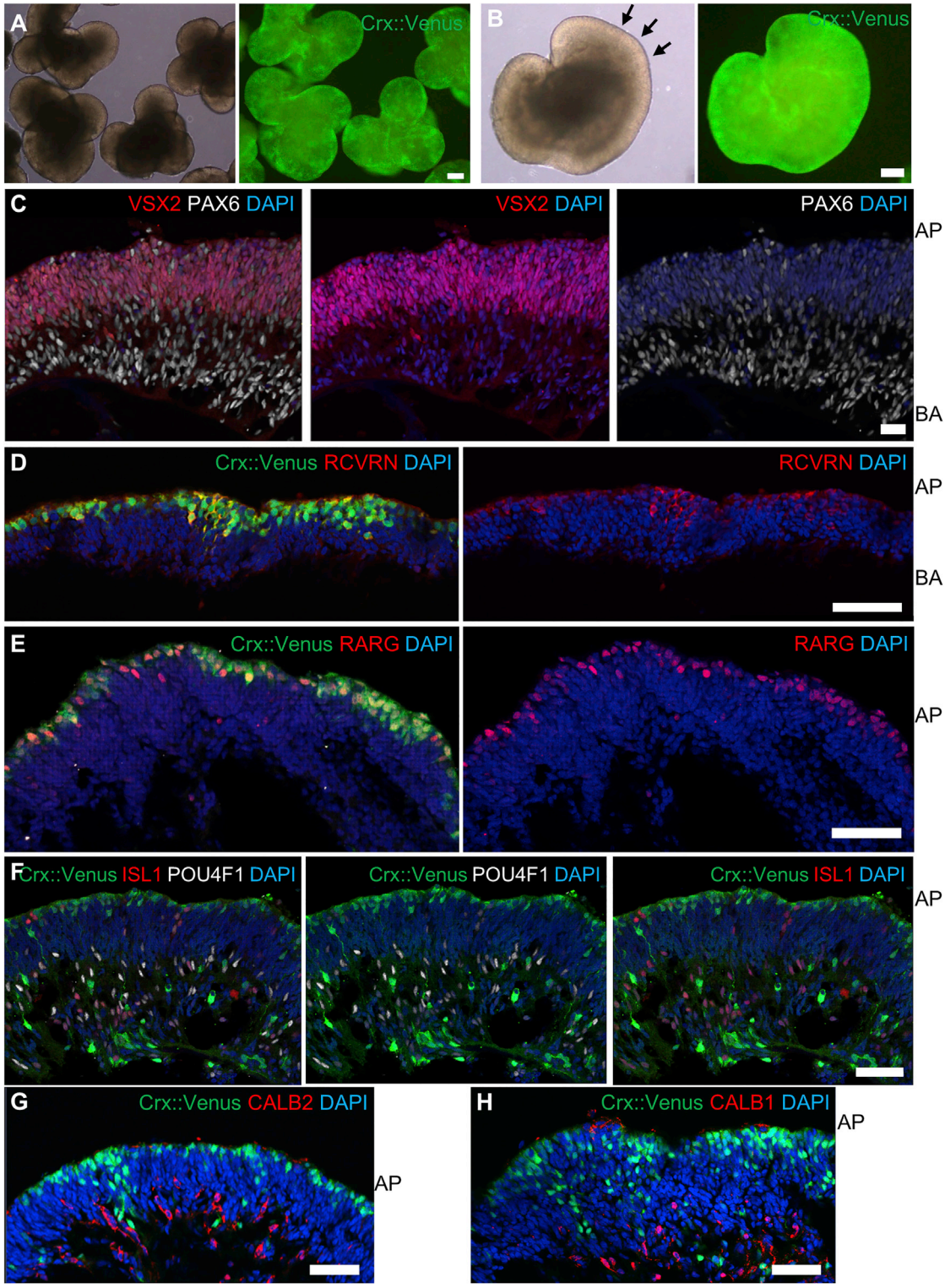

Figure 3. Expression of Early Retinal Markers in Crx::Venus Human ESC-Derived Retina before Transplantation

(A and B) hESC retinas were consistently differentiated into Crx::venus-positive optic vesicle-like tissues at DD60 (A) with characteristic continuous neural epithelium indicated by arrows (B).

(legend continued on next page)

immunoreactive for CD68, a lysosome-associated membrane protein, suggesting their pro-inflammatory nature (Figure 2D).

Since retinal degeneration is reported to be delayed in dark-reared *rd10* mice (Chang et al., 2007), retinal degeneration may have been accelerated by light in *rd10* with NOG background, as the NOG strain is albino and possibly more susceptible to light. Indeed, animals raised in the dark from day 17 of pregnancy showed delayed degeneration in both NOG-*rd10* and *rd10*, although the NOG strain still degenerated faster than the non-NOG strain (Figure S3B).

Absence of Immune Cells in Both NOG-rd and rd Mouse Retinas

We next studied the influence of the immune system upon retinal degeneration. Cytotoxic T cells, B cells, NK cells, and neutrophils in the retina were stained with anti-mouse CD8, CD19, NKp46 (NCR1), and LY6G antibodies, respectively (Figure S3C). The staining revealed no invasion by the aforementioned immune cells in the retina from any of these mouse lines at around the peak of retinal degeneration or inflammation (*rd1-2J* mice and NOG-*rd1-2J* mice on P14, *rd10* mice on P23, and NOG-*rd10* mice on P16).

In NOG-*rd10*, the expression of glial fibrillary acidic protein increased earlier than that of *rd10*, indicating the activated status of Müller cells during photoreceptor degeneration, and the expression pattern was similar between *rd1-2J* and NOG-*rd1-2J* (Figure S3D).

Differentiation and Characterization of Human ESC-Derived Retina

Retinal sheets for transplantation were prepared from hESCs (Crx::venus line), which were consistently differentiated into Crx::venus-positive retinas with a characteristic continuous neural epithelium formed by differentiation day 60 (DD60) (Figures 3A and 3B). These hESC retina had a layer of retinal progenitor cells positive for both PAX6 and Chx10 (VSX2) on the apical side with more differentiated PAX6-positive/Chx10-negative cells on the basal side (Figure 3C). Crx::venus-positive photoreceptor progenitor cells were observed on the apical margins, with some positive for the early photoreceptor marker Recoverin (RCVRN) and cone marker RxRγ (RARG) (Figures 3D and 3E). The presence of early-born cells including retinal ganglion cells (RGCs), amacrine cells, and horizontal cells are also suggested by the Brn3 (POU4F1), Islet1 (ISL1), calretinin (CALB2), and calbindin (CALB1) immunoreactivities (Figures 3F–3H).

Long-Term Survival and Maturation of Transplanted Human ESC-Derived Retina in NOG-*rd1-2J* Mice

Crx::venus hESC retinal sheets were transplanted at DD64–DD66 into the subretinal space of 8-week-old NOG-*rd1-2J* mouse eyes, which were collected for immunohistology at DD200–DD220, as we previously observed that hESC retina requires approximately 200 days to mature (Shirai et al., 2015). Human nuclei (HuNu)-positive hESC retina presented ONL with mature cones and rods as presented previously by us and others (Kaewkhaw et al., 2016; Shirai et al., 2015); Crx::venus- and rhodopsin-positive photoreceptors were in the organized rosette structures, wherein M/L and S cone opsins were usually present in larger Crx::venus-positive cells compared with rod photoreceptors, and localized at the inner and outer segment (IS/OS)-like structures (Figures 4A–4D). These IS/OS-like structures were also positive for peripherin-2 (PRPH2), a cell surface glycoprotein expressed in the OS (Figure 4E). We further characterized the ultrastructure of graft photoreceptor cells by electron microscopy and found components of mature photoreceptors such as mitochondria-rich IS, connecting cilia, and OS disc structures that were often sectioned obliquely (Figures 4F and 4G).

Other inner retinal cells were also present in transplants, as suggested by the immunoreactivities against PKCα (PRKCA, expressed exclusively in rod bipolar cells) and calretinin (expressed in amacrine and ganglion cells) (Figures S4A and S4B). Microglial cells of non-active ramified morphology were observed in the host retina and the graft, where they were often present inside the rosette of graft photoreceptors (Figures S4C and S4C′). Electron microscopy showed that these microglia were surrounded by oblique sections of OS disc-like structures, and some fractions of OS disc-like structures were engulfed by the microglia (Figures S4E–S4E″).

(C) Retinal progenitor cells positive for VSX2 (Chx10, red) and PAX6 (gray) are present on the apical side, while differentiated cells ($PAX6^+$/$VSX2^-$) are observed on the basal side.
(D and E) Crx::venus-positive cells are present on the apical side at DD60, with some of them co-labeled with (D) early photoreceptor marker RCVRN (Recoverin, red) and (E) early cone marker RARG (RxRγ, red).
(F) Presence of differentiated retinal ganglion cells and other inner cells on the basal side implied by ISL1 (Islet1, red) and POU4F1 (Brn3, gray) immunoreactivities.
(G) CALB2 (calretinin, red)-positive staining suggests the presence of amacrine, subtypes of ganglion, and horizontal cells.
(H) CALB1 (calbindin, red)-positive staining indicates the presence of horizontal cells and subtypes of ganglion cells.
AP, apical side; BA, basal side. Scale bars, 200 μm (A and B) and 50 μm (C–H).

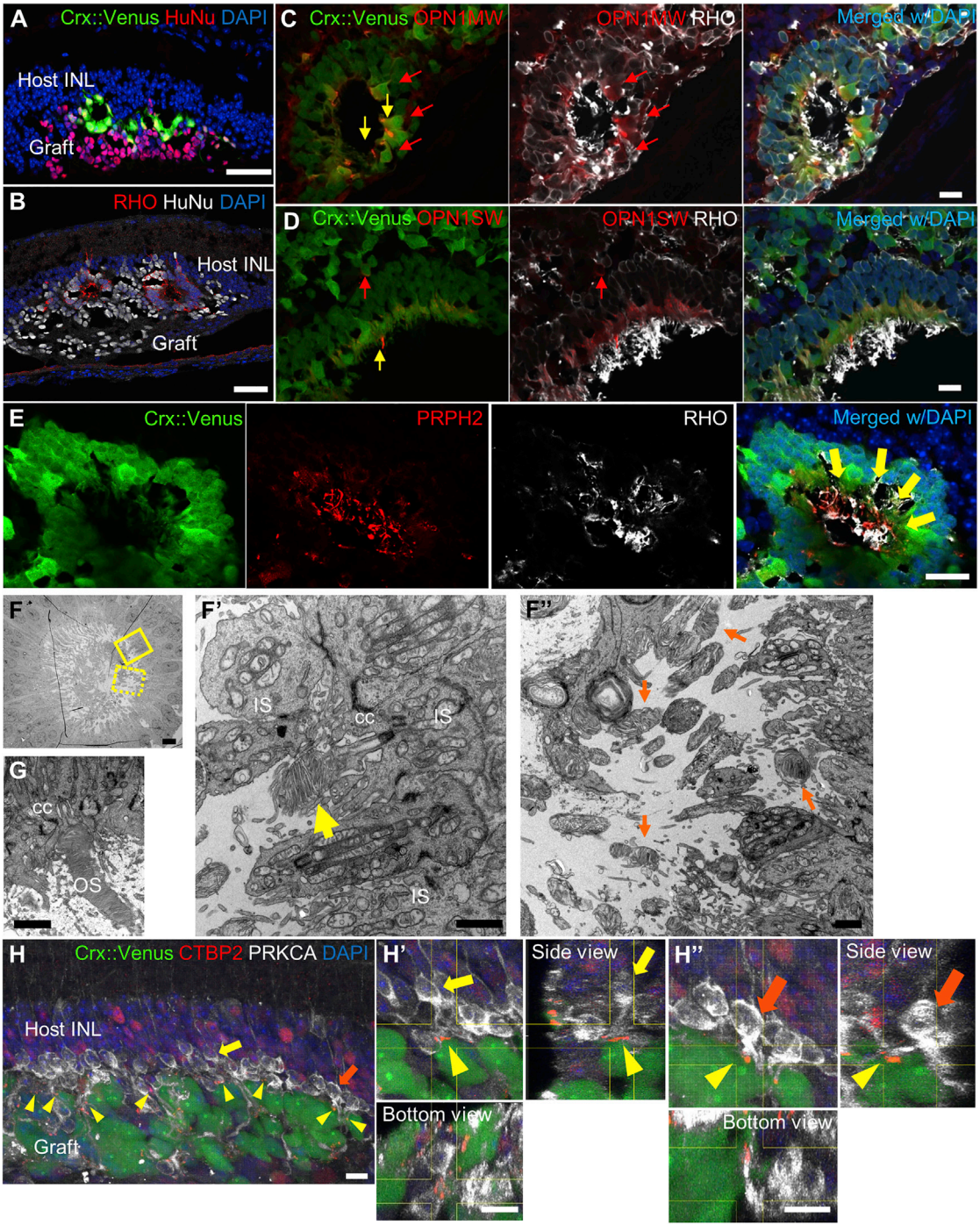

Figure 4. Expression of Maturation and Synapse Markers by Transplanted Crx::Venus hESC-Derived Retina in NOG-*rd1-2J* Mice

(A and B) Subretinal graft cells in the host NOG-*rd1-2J* mouse were positive for HuNu (human nuclei, red) staining, wherein the (A) Crx::venus (green)- or (B) rhodopsin-positive photoreceptors (red) formed organized rosette structures.

(C and D) M/L and S cone opsins were usually present in larger Crx::venus-positive cells (red arrows) compared with rod photoreceptors and sometimes localized in IS/OS-like structures (yellow arrows).

(E) Rod photoreceptor IS/OS formation was suggested by expression of PRPH2 (peripherin-2, red) inside the rosette-like structure (arrows).

(F and G) Graft cells in rosette-like structure show components of mature photoreceptors by electron microscopy. (F′) Higher magnification of solid line boxed area in (F) shows mitochondria-rich IS, connecting cilia (cc) and disrupted disc structures (yellow arrow); (F″) higher

(legend continued on next page)

At the host-graft interface, host bipolar cells were observed extending dendrites to Crx::venus-positive graft photoreceptors and the expression of RIBEYE, the synaptic ribbon-specific protein stained against CTBP2, was observed at the contact sites (Figure 4H and higher-magnification images in Figures 4H′ and 4H″). Müller glia in the host retina did not seem to block graft cell integration (Figure S4D).

Graft-Driven Light Responses Recorded in Host Retinal Neurons

Although *rd1* mice exhibit severe retinal degeneration with rod loss, cone cells can remain for weeks after rods have completely degenerated. We tested whether NOG-*rd1-2J* mouse retinas could elicit light responses at the time of transplantation (postnatal week 8). These retinas showed patchy, monolayered ONL and cone arrestin (ARR3) immunoreactivity in the distal retina but barely in the proximal area, with a similar trend observed in 12-week-old NOG-*rd1-2J* (Figure S5) retinas. We barely detected light responses from 8-week-old retinas (n = 4) but recorded a few responses in some 12-week-old retinas (n = 4, Figure S5D), again indicating the variability in the degree of cone degeneration. However, these responses were constrained to the distal retina, and no reaction was observed in the proximal area, defined as the area within 1-mm distance from the optic nerve disc.

Light-responsive RGCs of transplanted retinas were counted objectively and stringently, by only counting light responses observed as the same responsive pattern at least twice in the three repetitive recordings. Responses were further classified into either "normal responses" (transient-, brisk-sustained-, or sustained-ON; transient OFF; ON-OFF or sustained ON-OFF; ON suppression) or "hypersensitive" (ON-hyperactive; OFF-hyperactive; delayed-hyperactive) responses as previously described (Mandai et al., 2017). We previously reported that mouse iPSC (miPSC) retinal tissue can elicit light responses in host mouse RGCs (Mandai et al., 2017). In the present study, eight retinas were tested for light responses to full-field light stimuli at 12.84 log photons/cm^2/s (0.45 log cd/m^2/s, the same condition as in our previous report) by multi-electrode array (MEA) recording at 20–27 weeks after transplantation (DD200–DD260). While some samples showed none (3 of 8 retinas) or only weak or ambiguous light responses (2 of 8 retinas), evident light responses were recorded from three transplanted retinas in the proximal area (Figures 5 and 6).

MEA recording of one responding retina is presented in Figure 5 along with its corresponding *in vivo* images. At DD176, typical Crx::venus-positive rosette formation with no inflammatory signs, such as increased vascular permeability or leakage of fluorescein dye at the graft site, was confirmed by angiography (Figure 5A). The same retina was recorded by the MEA system at DD204, and the representative peri-stimulus time histogram (PSTH) demonstrates the RGC spikes in each recording channels after recovery from the ON pathway blocker (L-AP4; 20 μM) application (Figures 5B and 5C). Overall, 11 RGCs were recorded with "normal" responses (4 transient ON; 2 sustained ON-OFF; 2 brisk-sustained ON; 3 sustained ON) and 13 RGCs with hypersensitive response (13 ON-hypersensitive) after 9-*cis*-retinal replenishment. In the presence of L-AP4, only 11 RGCs with hypersensitive responses were detected (9 ON-hyperactive; 2 delayed-hyperactive). After washout, normal responses were again detected in nine RGCs (4 transient ON; 2 brisk-sustained ON; 3 sustained ON) while 11 RGCs showed hypersensitive responses (9 ON-hyperactive; 2 delayed-hyperactive) (Figure 5D). The "normal responses" as clustered by our program resembled those of wild-type RGCs in response to L-AP4, and increased along with stimulus intensity changes, whereas some hypersensitive responses did not change with or without L-AP4 (Figure 5E). The subsequent whole-mount immunostaining strongly suggests the host RGC origin of "normal" light responses over the mature graft area, where host bipolar cell contacts with the graft photoreceptors are indicated by RIBEYE staining (Figures 5F and 5G).

Two other samples that showed light-responsive RGC activities indicative of graft origin are presented in Figure 6. One sample showed clear light responses only after L-AP4 washout over the graft area (Figure 6A). The other sample showed RGC responses even before 9-*cis*-retinal treatment, and the number of light-responsive RGCs decreased upon L-AP4 treatment but increased again after washout, although classified as hypersensitive patterns (6 ON-hyperactive) (Figure 6B).

magnification of dotted line boxed area in (F) shows many fragments of disc structures inside the rosette on an oblique section (orange arrows). (G) Continuous view of connecting cilia and OS from a cell body in another section of the same rosette.
(H) 3D confocal image of transplanted area stained against CTBP2 (RIBEYE as presynaptic marker, arrowheads) and PRKCA (PKCα as rod bipolar cell marker, gray). CTBP2 was co-localized at the contact site of graft photoreceptors (green) and host bipolar cells that can be traced back into the host retina (yellow and orange arrows). (H′ and H″) The views indicated by arrows are the representative contact sites, and magnified views are presented as projected optical section and orthogonal views between the indicated lines.
INL, inner nuclear layer; IS, inner segment; OS, outer segment. DD200–DD220 (A–D). Scale bars, 50 μm (A and B), 20 μm (C–E), 5 μm (F), 1 μm (F′–G), and 10 μm (H–H″).

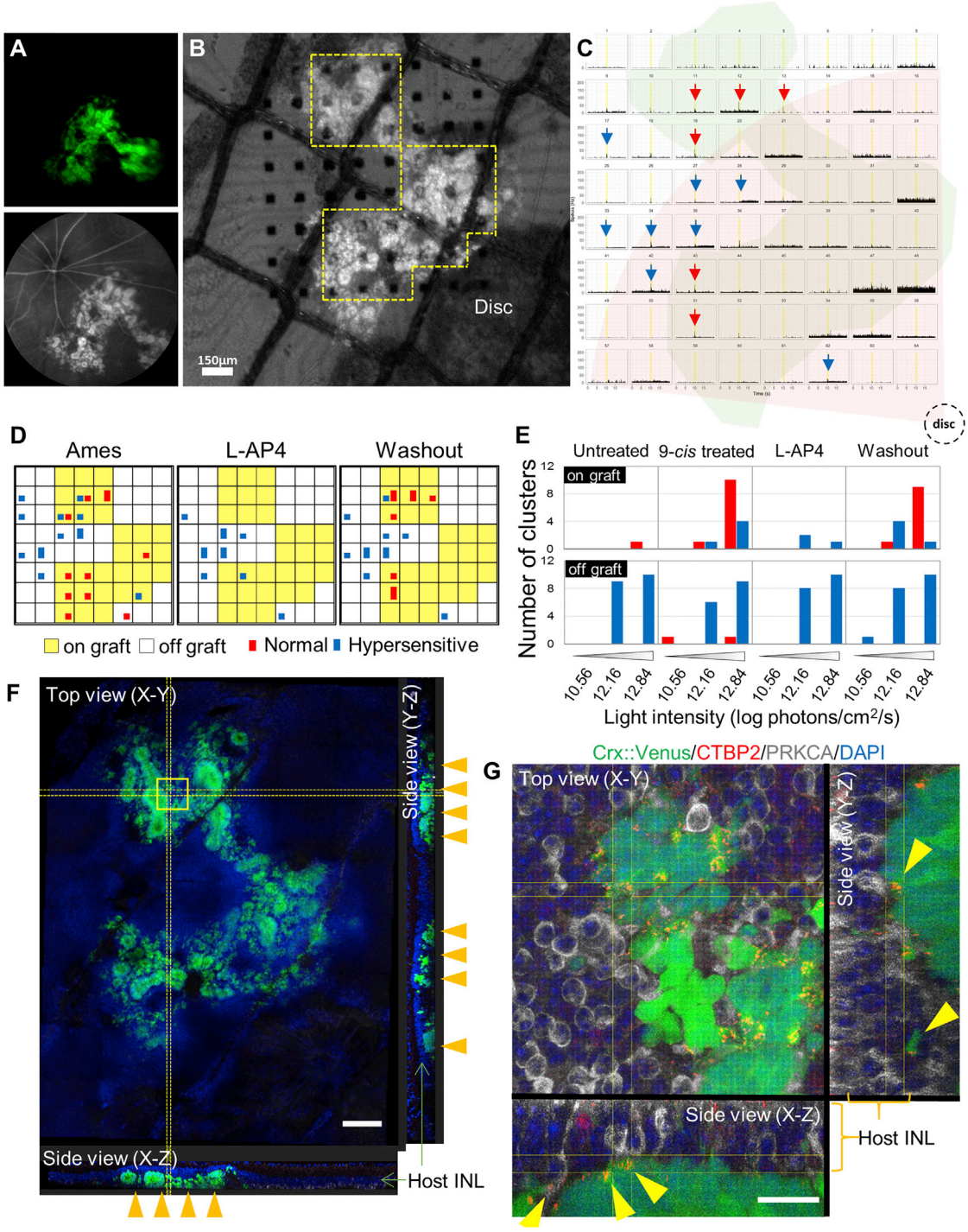

Figure 5. Classic Photoreceptor Responses Elicited in NOG-*rd1-2J* Mouse after Transplantation of hESC-Derived Retina

(A) *In vivo* imaging of a transplanted eye at postoperative day 112 (DD176). Fluorescent angiography shows the Crx::venus-positive graft under the retinal vessels. No sign of rejection was observed.

(B) Isolated retina from (A) with Crx::venus hESC-derived graft (DD204) mounted on the MEA probe with RGC on the electrodes side.

(C) Averaged peri-stimulus time histogram of RGC spikes (after spike sorting) against three repeated mesopic light stimuli (12.84 log photons/cm^2/s) after washout of L-AP4. Yellow bars indicate the 1-s light stimulation. Red and blue arrows indicate the channels with the

(legend continued on next page)

In two other samples, the number of light-responsive RGCs was so few on the graft that we could not conclusively determine the origin of the responses. In the rest of the three samples only a small fraction of the graft was laid on the electrodes, and no RGC responses were detected.

To test whether NOG-*rd1-2J* mice are as adequate and competent to accept retina transplants as *rd1-2J* mice in our previous study, we also transplanted miPSC retina (Nrl-GFP/ROSA:Nrl-CtBP2-tdTomato iPSC line) (Mandai et al., 2017) at the same age as the hESC retina recipient NOG-*rd1-2J* mice. After 5 weeks of transplantation, evident microERG (mERG) responses were consistently recorded over the graft area in all the transplanted samples as well as typical RGC light responses sensitive to L-AP4 (n = 4) (Figure 7).

DISCUSSION

In this study, we established two immunodeficient retinal degeneration model mouse strains, NOG-*rd1-2J* and NOG-*rd10*, for transplantation of human retinal cells or tissue. Initially, our goal was to obtain two model lines with different degeneration speeds. However, degeneration was unexpectedly fast in NOG-*rd10* mice in comparison with *rd10* mice. In these NOG backgrounds, immune cells such as T cells, B cells, and NK cells were markedly reduced, whereas microglia were similarly present compared with non-NOG mice. We did not observe infiltration of these T, B, or NK cells in the retina during the photoreceptor degeneration in either *rd1-2J* or *rd10* mice, even though these mouse lines both possess an intact immune system. There are controversial reports about the role of microglia in retinal degeneration (Arroba et al., 2011; Jin et al., 2016; Peng et al., 2014). We observed microglia infiltration into ONL after the detection of initial apoptosis marker appearance in photoreceptor cells, both in NOG-*rd10* and *rd10* mice. Although some reported that T cells could influence microglia to be neurotoxic or neurotrophic (González et al., 2014), the lack of T cell infiltration argues against this mechanism. The pro-inflammatory phenotype of microglia indicated by CD68 staining was similarly observed in both *rd10* and NOG-*rd10* mice. It was reported that different inbred strains showed markedly different sensitivities to light (LaVail et al., 1987). Since retinas from dark-reared *rd10* mice exhibited delayed degeneration onset while dark rearing had no effect on *rd1-2J* retinal degeneration (Chang et al., 2007), sensitivity to light may affect the pathology of *rd10* mice. In our study, since degeneration in both *rd10* and NOG-*rd10* mice was slowed down when dark-reared, in addition to light effect, the immunodeficiency or other genetic differences between the different strain backgrounds may have also accelerated the degeneration.

We experienced difficulties in observing maturation of hESC retinas in *rd1* mice even with immunosuppression, but with NOG-*rd1-2J* mice the transplanted hESC retinas consistently developed mature ONL with rod and cone opsins. Furthermore, graft photoreceptors show signs of developing IS/OS structures as evidenced by electron microscopy. However, we had not yet shown any function by hESC/iPSC retina following transplantation. In the present study, light-responsive RGC activities were detected in 3 of 8 retinas over the grafts by MEA recording from 28-week-old or older NOG-*rd1-2J* mice (20 weeks or more after transplantation). At such advanced stage of retinal degeneration or even younger NOG-*rd1-2J*, no remaining cone activity was observed in the proximal retina where the grafts usually lay. Although we could not completely deny the rescue effect on the host's remaining cones by grafts, some of the light responses recorded after transplantation were clearly distinguished by their proximity to the disc and location directly over the graft. These responses were not sparsely covering only a few electrodes as in the non-transplanted retina but were detected in clusters covering multiple electrodes directly in the grafted area, suggesting that they are more likely

RGCs showing normal and hypersensitive responses, respectively. The proximal retina (<1 mm from disc) is indicated in pink, and the area covered by the graft is shown in light green.
(D) Spatial distribution of the RGC numbers (spike sources) shown as normal (red bars) or hypersensitive (blue bars) in accordance with the 64 electrodes, ranging from 1 to 2 cells per channel. Electrodes covered by the graft are shown in yellow.
(E) Histogram of total RGC cluster numbers in electrodes covering grafted (on graft) or non-grafted (off graft) areas. RGC with normal responses (red) in grafted areas increased along with stimulus intensity and were abolished in the presence of L-AP4. Hypersensitive responses (blue) in non-grafted areas were insensitive to L-AP4. Stimulus intensities are shown in log photons/cm^2/s.
(F) Overview of the retinal sheet after MEA recording shown in (B). Transplanted grafts were distributed in the subretinal area (orange arrowheads).
(G) Magnified view of a light-responsive area (yellow box in F, around channel 12 in C). Yellow arrowheads mark the potential synaptic connections between host rod bipolar cells (PKCα-positive) and graft Crx::venus-positive photoreceptor cells expressing synaptic ribbon proteins (CTBP2-positive).
Scale bars, 150 μm (F) and 20 μm (G).

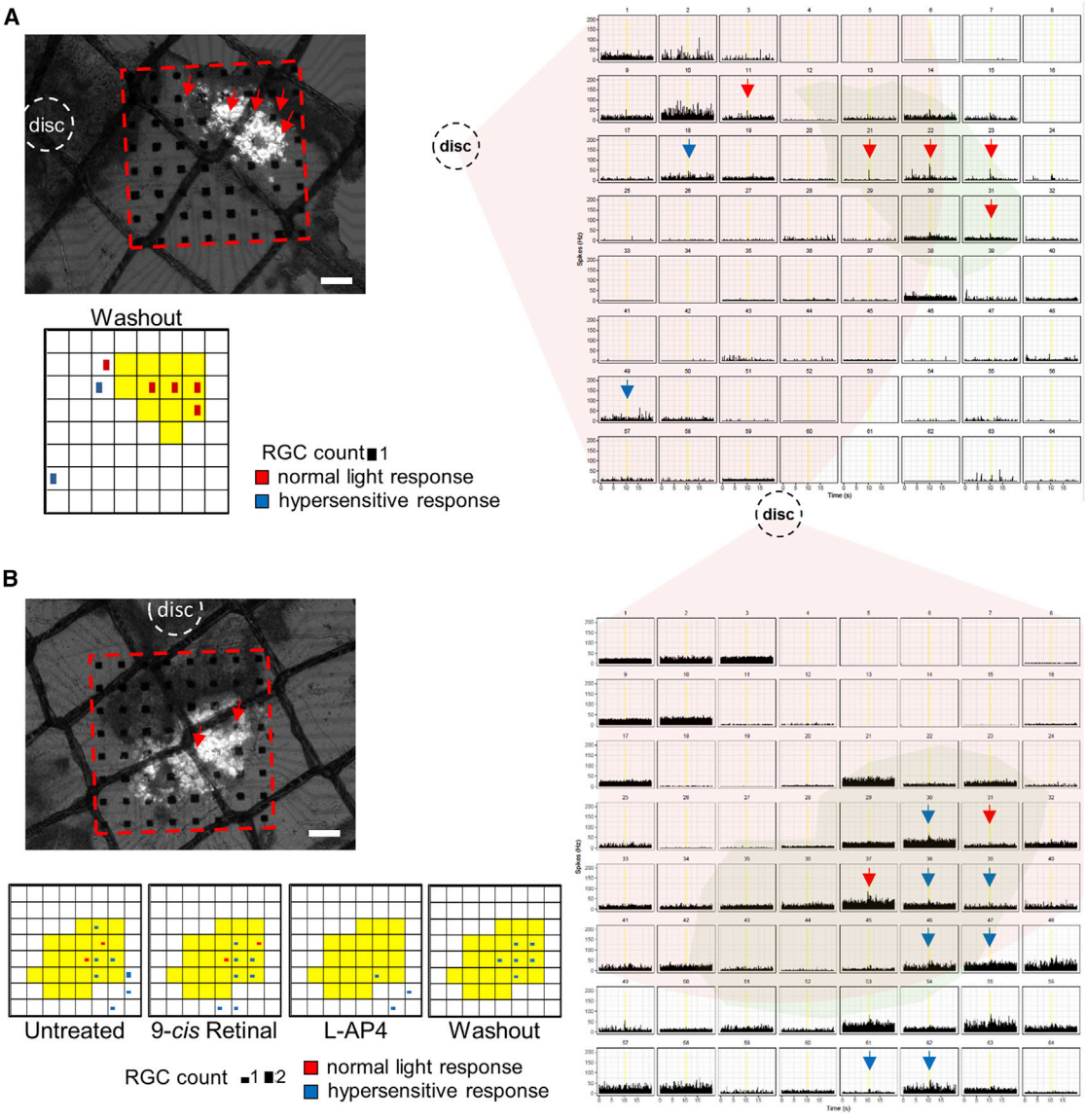

Figure 6. Light Responses in the Proximal Retinas of hESC-Retina Transplanted NOG-*rd1-2J* Mice

Examples of the other two transplanted retinas with light-driven RGC responses detected by MEA recording. Light responses are marked by arrows in red for normal and blue for hypersensitive responses. Red dotted boxes indicate the electrode areas. The proximal retina (within 1 mm from disc) is indicated in pink shadow, and the area covered by graft in green shadow.

(A) A sample with evident light responses. The response was evident only after L-AP4 washout against mesopic light stimuli (12.84 log photons/cm^2/s).

(B) Another sample with RGCs with light responses before and after 9-*cis*-retinal and L-AP4 treatment with mesopic light stimuli.

Scale bars, 150 μm.

driven by the graft photoreceptors rather than remaining cones.

Hypersensitive response patterns were initially observed in the degenerating retinas, preferentially to a bright light stimulus but barely with our regular light stimuli at 0.45 log cd/m^2/s (Mandai et al., 2017). After transplantation, however, many RGCs, usually located in and around the grafted area, were classified as "light-responsive hypersensitive" even to the regular light stimuli. Some of the hypersensitive responses were rather ambiguous as they cannot be clearly distinguished from the normal patterns, such as whether to be sustained ON or ON-hyperactive. We propose that these patterns represent either degenerating or regenerating processes and may possibly originate from the

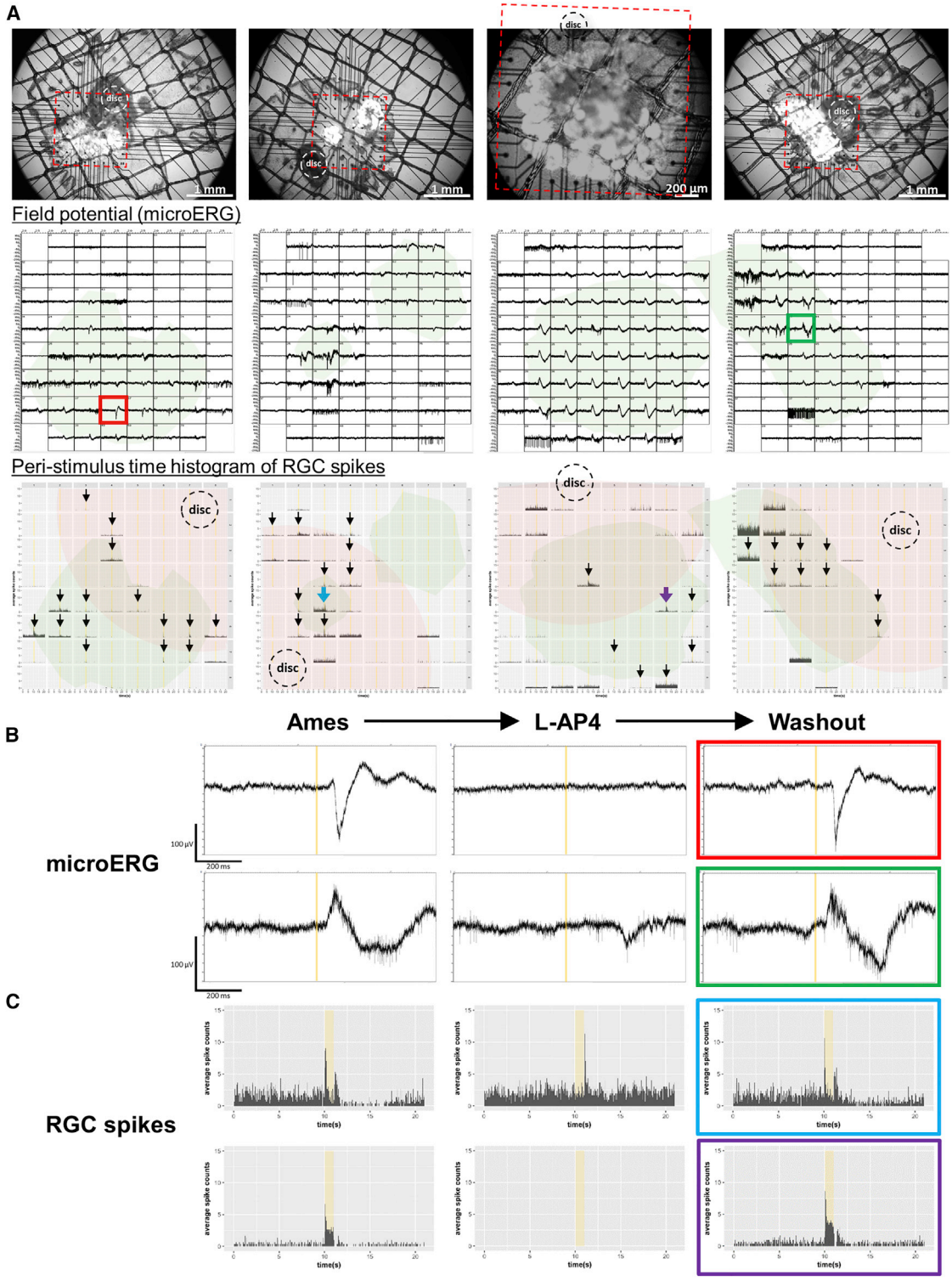

Figure 7. mERG and RGC Responses Elicited in NOG-*rd1-2J* Mice after miPSC-Retina Transplantation

(A) mERG recordings and representative peri-stimulus time histogram after L-AP4 washout and spike sorting are presented along with images of miPSC retina transplants mounted on the MEA probe (60MEA200/30iR-Ti-gr, n = 4). Electrodes with light-responsive RGCs are indicated by arrows. Recording areas are indicated by red dotted line boxes. The proximal retinas (within 1 mm from disc) are indicated in pink, with the areas covered by the grafts in green.

(legend continued on next page)

immature host-graft synaptic connections or cells associated with the circuitry formation. No OFF responses were detected upon L-AP4 block, suggesting that the OFF pathway may not yet have been recovered. The L-AP4-insensitive hypersensitive activities may be partly derived from intrinsically photosensitive RGCs, despite the use of Opsinamide. Alternatively, these responses may suggest a wrongly or immaturely rewired circuitry tethered to the rather excitable RGCs in degenerating retina (Euler and Schubert, 2015). It is noteworthy that we obtained light responses in one sample even before the 9-*cis*-retinal treatment (Figure 6B), which indicates that graft photoreceptors were readily functional with functional visual pigments *in vivo*, even though the rosette formation dampens normal contact with RPE cells.

In the present study, we did not detect full-field ERG response after transplantation. Since detectable ERG response is estimated to require more than 150,000-cell integration (Pearson et al., 2012), our host-graft integration is not considered to be sufficient. However, considering that a patient with non-recordable full-field ERG still has a limited visual field, the absence of *in vivo* full-field ERG does not indicate total blindness. For the *ex vivo* recording, although the evident mERGs were elicited in miPSC retina grafts at 5 weeks after transplantation, we did not detect mERG in hESC retina grafts to the same 10-ms flashlight (1/100 photons compared with the multiunit recordings of RGC). Since the mERG responses in miPSC were mostly abolished by L-AP4, the wave components likely represented the postsynaptic bipolar cells and RGCs of either graft or host rather than the properly oriented photoreceptors of limited amount inside the graft rossettes (Fujii et al., 2016). The lack of mERG wave components but not RGC multiunit responses in hESC retina suggests that the graft photoreceptors did not convey a strong enough response to the weaker stimulus. Still, we obtained RGC responses in 3 of 7 retinas with a substantial hESC transplant, which suggests the presence of functional hESC retinal photoreceptors, although RGC responses were detected in all samples from miPSC retina-transplanted NOG-*rd1-2J* mice. The lower responsiveness of hESC retina compared with miPSC retina in NOG-*rd1-2J* mice may be attributed to (1) fewer functional photoreceptors in hESC retina than in miPSC retina, (2) the advanced and aged host environment at the time of synaptic integration of hESC retinas, since hESC retina takes a longer time to reach synaptogenesis stage than does miPSC retina, and (3) inefficient synaptic formation in xenotransplantation compared with allotransplantation as suggested by Laver and Matsubara (2017). However, this incompatibility of hESC/iPSC retina would not be an issue in human host retinas. Finally, (4) the Crx::venus ESC graft we have used here may have negatively affected synaptogenesis, since functional maturation is reportedly delayed in $Crx^{+/-}$ mice (Furukawa et al., 1999).

In summary, by introducing immune-deficient end-stage rd mouse models, we were able to integrate hESC retinal sheets in the transplanted retinas for an extended period. These grafts showed signs of photoreceptor maturation including light-responsive IS/OS formation and synaptogenesis, and tentative functional integration with host retina, albeit to an extent less than with allotransplantation. This study supports the use of these animals in preclinical studies, as well as the competency of hESC retina for future clinical applications in RP patients.

EXPERIMENTAL PROCEDURES

All animal experiments were conducted in accordance with local guidelines and the ARVO statement on the use of animals in ophthalmic and vision research. All experimental protocols were approved by the committee of the RIKEN Center for Developmental Biology.

Development of NOG-*rd1-2J* and NOG-*rd10* Mice

To establish two types of NOG-rd transgenic mice, we used marker-assisted screening methods (Figure 1A). Details are described, with genotyping information, in Supplemental Experimental Procedures.

hESC-Derived Retina Differentiation and Subretinal Transplantation

Human ESCs (KhES-1 line) were cultured in accordance with the hESC research guidelines of the Japanese government. The hESC reporter line (Crx::venus) was maintained and differentiated as previously described with a slight modification (Kuwahara et al., 2017; Nakano et al., 2012; Shirai et al., 2015). Human ESC retinal sheets were transplanted at DD64–DD66 as described previously (Assawachananont et al., 2014; Shirai et al., 2015). Details are provided in Supplemental Experimental Procedures.

Details for animal sources and methods for *in vivo* electroretinogram and ocular imaging, electron microscopy, miPSC retina transplantation, and immunohistochemistry with antibody information are included in Supplemental Experimental Procedures.

(B) Representative mERG in the red- and green-boxed channels in (A). L-AP4 abolished the negative wave (RGC response, red box) or the positive wave (ON bipolar response, green box).
(C) L-AP4-sensitive ON suppression (blue) and sustained-ON responses (purple) are shown as representative RGC responses in the channels pointed out by blue and purple arrows in (A).

SUPPLEMENTAL INFORMATION

Supplemental Information includes Supplemental Experimental Procedures, five figures, four tables, and one data file and can be found with this article online at https://doi.org/10.1016/j.stemcr.2018.01.032.

AUTHOR CONTRIBUTIONS

M.M. and M.T. designed and supervised the study. S.I. conducted the analysis on NOG-rd mice. H.-Y.T., M.F., and T.M. conducted and analyzed MEA. S.I., H.-Y.T., and M.M. performed 3D image analysis. N.K., T.K., M.G., and R.T. planned and established NOG-rd mice. S.S. performed immunological analysis of NOG-rd mice. G.A.S. supervised modeling and analysis of retinal degeneration. S. Yamasaki, A. Kuwahara, and A. Kishino prepared and characterized hESC retinas. T.W. performed *in vivo* experiments/analysis. S. Yonemura provided data on electron microscopy. S.I., H.-Y.T., M.M., M.E., and H.T. analyzed and interpreted the data. S.I., H.-Y.T., G.A.S., and M.M. wrote the manuscript. All authors reviewed and approved the final manuscript.

ACKNOWLEDGMENTS

We thank Kenji Sakamoto at Kitasato University for supplying *rd1-2J* mice and Hanako Ikeda at Kyoto University for supplying *rd10* mice for relocating procedure under Jackson's approval. We thank Tomoyo Hashiguchi, Yoshiko Takahashi, Junki Sho, Shoko Fujino, and Naoko Hayashi for technical support and members of the M.T. laboratory for discussions. S.I. was supported by the fellowship of Junior Research Associate (JRA) from RIKEN. This study was supported by AMED under grant number 17bm0204002h0005. S. Yamasaki, A. Kuwahara, and A. Kishino are employees of Sumitomo Dainippon Pharma; this work was supported in part by a grant from Sumitomo Dainippon Pharma.

Received: June 29, 2017
Revised: January 28, 2018
Accepted: January 29, 2018
Published: March 1, 2018

REFERENCES

Arroba, A.I., Álvarez-Lindo, N., van Rooijen, N., and de la Rosa, E.J. (2011). Microglia-mediated IGF-I neuroprotection in the rd10 mouse model of retinitis pigmentosa. Invest. Ophthalmol. Vis. Sci. *52*, 9124–9130.

Assawachananont, J., Mandai, M., Okamoto, S., Yamada, C., Eiraku, M., Yonemura, S., Sasai, Y., and Takahashi, M. (2014). Transplantation of embryonic and induced pluripotent stem cell-derived 3D retinal sheets into retinal degenerative mice. Stem Cell Reports *2*, 662–674.

Barnea-Cramer, A.O., Wang, W., Lu, S.J., Singh, M.S., Luo, C., Huo, H., McClements, M.E., Barnard, A.R., MacLaren, R.E., and Lanza, R. (2016). Function of human pluripotent stem cell-derived photoreceptor progenitors in blind mice. Sci. Rep. *6*, 29784.

Chang, B., Hawes, N.L., Pardue, M.T., German, A.M., Hurd, R.E., Davisson, M.T., Nusinowitz, S., Rengarajan, K., Boyd, A.P., Sidney, S.S., et al. (2007). Two mouse retinal degenerations caused by missense mutations in the β-subunit of rod cGMP phosphodiesterase gene. Vis. Res. *47*, 624–633.

Cuenca, N., Fernández-Sánchez, L., Campello, L., Maneu, V., De la Villa, P., Lax, P., and Pinilla, I. (2014). Cellular responses following retinal injuries and therapeutic approaches for neurodegenerative diseases. Prog. Retin. Eye Res. *43*, 17–75.

Decembrini, S., Koch, U., Radtke, F., Moulin, A., and Arsenijevic, Y. (2014). Derivation of traceable and transplantable photoreceptors from mouse embryonic stem cells. Stem Cell Reports *2*, 853–865.

Eiraku, M., Takata, N., Ishibashi, H., Kawada, M., Sakakura, E., Okuda, S., Sekiguchi, K., Adachi, T., and Sasai, Y. (2011). Self-organizing optic-cup morphogenesis in three-dimensional culture. Nature *472*, 51–56.

Euler, T., and Schubert, T. (2015). Multiple independent oscillatory networks in the degenerating retina. Front. Cell. Neurosci. *9*, 444.

Fujii, M., Sunagawa, G.A., Kondo, M., Takahashi, M., and Mandai, M. (2016). Evaluation of micro electroretinograms recorded with multiple electrode array to assess focal retinal function. Sci. Rep. *6*, 30719.

Furukawa, T., Morrow, E.M., Li, T., Davis, F.C., and Cepko, C.L. (1999). Retinopathy and attenuated circadian entrainment in Crx-deficient mice. Nat. Genet. *23*, 466–470.

González, H., Elgueta, D., Montoya, A., and Pacheco, R. (2014). Neuroimmune regulation of microglial activity involved in neuroinflammation and neurodegenerative diseases. J. Neuroimmunol. *274*, 1–13.

Gonzalez-Cordero, A., West, E.L., Pearson, R.A., Duran, Y., Carvalho, L.S., Chu, C.J., Naeem, A., Blackford, S.J.I., Georgiadis, A., Lakowski, J., et al. (2013). Photoreceptor precursors derived from three-dimensional embryonic stem cell cultures integrate and mature within adult degenerate retina. Nat. Biotechnol. *31*, 741–747.

Guo, C., Otani, A., Oishi, A., Kojima, H., Makiyama, Y., Nakagawa, S., and Yoshimura, N. (2012). Knockout of ccr2 alleviates photoreceptor cell death in a model of retinitis pigmentosa. Exp. Eye Res. *104*, 39–47.

Hambright, D., Park, K.Y., Brooks, M., McKay, R., Swaroop, A., and Nasonkin, I.O. (2012). Long-term survival and differentiation of retinal neurons derived from human embryonic stem cell lines in un-immunosuppressed mouse retina. Mol. Vis. *18*, 920–936.

Ito, M., Hiramatsu, H., Kobayashi, K., Suzue, K., Kawahata, M., Hioki, K., Ueyama, Y., Koyanagi, Y., Sugamura, K., Tsuji, K., et al. (2002). NOD/SCID/gamma(c)(null) mouse: an excellent recipient mouse model for engraftment of human cells. Blood *100*, 3175–3182.

Jin, N., Gao, L., Fan, X., and Xu, H. (2016). Friend or foe? Resident microglia vs bone marrow-derived microglia and their roles in the retinal degeneration. Mol. Neurobiol. *54*, 4094–4112.

Kaewkhaw, R., Swaroop, M., Homma, K., Nakamura, J., Brooks, M., Kaya, K.D., Chaitankar, V., Michael, S., Tawa, G., Zou, J., et al. (2016). Treatment paradigms for retinal and macular diseases using 3-d retina cultures derived from human reporter pluripotent stem cell lines. Invest. Ophthalmol. Vis. Sci. *57*, ORSFl1–ORSFl11.

Kanemura, H., Go, M.J., Shikamura, M., Nishishita, N., Sakai, N., Kamao, H., Mandai, M., Morinaga, C., Takahashi, M., and

Kawamata, S. (2014). Tumorigenicity studies of induced pluripotent stem cell (iPSC)-derived retinal pigment epithelium (RPE) for the treatment of age-related macular degeneration. PLoS One *9*, e85336.

Kim, K.H., Puoris'haag, M., Maguluri, G.N., Umino, Y., Cusato, K., Barlow, R.B., and de Boer, J.F. (2008). Monitoring mouse retinal degeneration with high-resolution spectral-domain optical coherence tomography. J. Vis. *8*, 17.1–17.11.

Kuwahara, A., Nakano, T., and Eiraku, M. (2017). Generation of a three-dimensional retinal tissue from self-organizing human ESC culture. Methods Mol. Biol. *1597*, 17–29.

Lamba, D.A., Gust, J., and Reh, T.A. (2009). Transplantation of human embryonic stem cell-derived photoreceptors restores some visual function in Crx-deficient mice. Cell Stem Cell *4*, 73–79.

Larsson, L.C., Czech, K.A., Brundin, P., and Widner, H. (2000). Intrastriatal ventral mesencephalic xenografts of porcine tissue in rats: immune responses and functional effects. Cell Transplant. *9*, 261–272.

LaVail, M.M., Gorrin, G.M., Repaci, M.A., Thomas, L.A., and Ginsberg, H.M. (1987). Genetic regulation of light damage to photoreceptors. Invest. Ophthalmol. Vis. Sci. *28*, 1043–1048.

Laver, C.R.J., and Matsubara, J.A. (2017). Structural divergence of essential triad ribbon synapse proteins among placental mammals—implications for preclinical trials in photoreceptor transplantation therapy. Exp. Eye Res. *159*, 156–167.

Machida, K., Suemizu, H., Kawai, K., Ishikawa, T., Sawada, R., Ohnishi, Y., and Tsuchiya, T. (2009). Higher susceptibility of NOG mice to xenotransplanted tumors. J. Toxicol. Sci. *34*, 123–127.

Mandai, M., Fujii, M., Hashiguchi, T., Sunagawa, G.A., Ito, S.I., Sun, J., Kaneko, J., Sho, J., Yamada, C., and Takahashi, M. (2017). iPSC-derived retina transplants improve vision in rd1 end-stage retinal-degeneration mice. Stem Cell Reports *8*, 1112–1113.

Mishra, A., Das, B., Nath, M., Iyer, S., Kesarwani, A., Bhattacharjee, J., Arindkar, S., Sahay, P., Jain, K., Sahu, P., et al. (2017). A novel immunodeficient NOD.SCID *-rd1* mouse model of retinitis pigmentosa to investigate potential therapeutics and pathogenesis of retinal degeneration. Biol. Open *6*, 449–462.

Nakano, T., Ando, S., Takata, N., Kawada, M., Muguruma, K., Sekiguchi, K., Saito, K., Yonemura, S., Eiraku, M., and Sasai, Y. (2012). Self-formation of optic cups and storable stratified neural retina from human ESCs. Cell Stem Cell *10*, 771–785.

Noailles, A., Maneu, V., Campello, L., Gómez-Vicente, V., Lax, P., and Cuenca, N. (2016). Persistent inflammatory state after photoreceptor loss in an animal model of retinal degeneration. Sci. Rep. *6*, 33356.

Pearson, R.A., Barber, A.C., Rizzi, M., Hippert, C., Xue, T., West, E.L., Duran, Y., Smith, A.J., Chuang, J.Z., Azam, S.A., et al. (2012). Restoration of vision after transplantation of photoreceptors. Nature *485*, 99–103.

Pearson, R.A., Gonzalez-Cordero, A., West, E.L., Claudio Ribeiro, J.R., Aghaizu, N., Goh, D., Sampson, R.D., Georgiaids, A., Waldron, P.V., Duran, Y., et al. (2016). Donor and host photoreceptors engage in material transfer following transplantation of postmitotic photoreceptor precursors. Nat. Commun. *7*, 13029.

Peng, B., Xiao, J., Wang, K., So, K.F., Tipoe, G.L., and Lin, B. (2014). Suppression of microglial activation is neuroprotective in a mouse model of human retinitis pigmentosa. J. Neurosci. *34*, 8139–8150.

Pennesi, M.E., Michaels, K.V., Magee, S.S., Maricle, A., Davin, S.P., Garg, A.K., Gale, M.J., Tu, D.C., Wen, Y., Erker, L.R., et al. (2012). Long-term characterization of retinal degeneration in rd1 and rd10 mice using spectral domain optical coherence tomography. Invest. Ophthalmol. Vis. Sci. *53*, 4644–4656.

Rohrer, B., Demos, C., Frigg, R., and Grimm, C. (2007). Classical complement activation and acquired immune response pathways are not essential for retinal degeneration in the rd1 mouse. Exp. Eye Res. *84*, 82–91.

Santos-Ferreira, T., Llonch, S., Borsch, O., Postel, K., Haas, J., and Ader, M. (2016a). Retinal transplantation of photoreceptors results in donor–host cytoplasmic exchange. Nat. Commun. *7*, 13028.

Santos-Ferreira, T., Völkner, M., Borsch, O., Haas, J., Cimalla, P., Vasudevan, P., Carmeliet, P., Corbeil, D., Michalakis, S., Koch, E., et al. (2016b). Stem cell-derived photoreceptor transplants differentially integrate into mouse models of cone-rod dystrophy. Invest. Ophthalmol. Vis. Sci. *57*, 3509–3520.

Seiler, M.J., Aramant, R.B., Jones, M.K., Ferguson, D.L., Bryda, E.C., and Keirstead, H.S. (2014). A new immunodeficient pigmented retinal degenerate rat strain to study transplantation of human cells without immunosuppression. Graefes Arch. Clin. Exp. Ophthalmol. *252*, 1079–1092.

Seiler, M.J., Lin, R.E., McLelland, B.T., Mathur, A., Lin, B., Sigman, J., De Guzman, A.T., Kitzes, L.M., Aramant, R.B., and Thomas, B.B. (2017). Vision recovery and connectivity by fetal retinal sheet transplantation in an immunodeficient retinal degenerate rat model. Invest. Ophthalmol. Vis. Sci. *58*, 614–630.

Shirai, H., Mandai, M., Matsushita, K., Kuwahara, A., Yonemura, S., Nakano, T., Assawachananont, J., Kimura, T., Saito, K., Terasaki, H., et al. (2015). Transplantation of human embryonic stem cell-derived retinal tissue in two primate models of retinal degeneration. Proc. Natl. Acad. Sci. USA *113*, E81–E90.

Singh, M.S., Balmer, J., Barnard, A.R., Aslam, S.A., Moralli, D., Green, C.M., Barnea-Cramer, A., Duncan, I., and MacLaren, R.E. (2016). Transplanted photoreceptor precursors transfer proteins to host photoreceptors by a mechanism of cytoplasmic fusion. Nat. Commun. *7*, 13537.

Tucker, B.A., Park, I.H., Qi, S.D., Klassen, H.J., Jiang, C., Yao, J., Redenti, S., Daley, G.Q., and Young, M.J. (2011). Transplantation of adult mouse iPS cell-derived photoreceptor precursors restores retinal structure and function in degenerative mice. PLoS One *6*, e18992.

Watanabe, S., Terashima, K., Ohta, S., Horibata, S., Yajima, M., Shiozawa, Y., Dewan, M.Z., Yu, Z., Ito, M., Morio, T., et al. (2011). Specific humoral immune responses Hematopoietic stem cell-engrafted NOD/SCID/IL2Rg null mice develop human lymphoid systems and induce long-lasting HIV-1 infection with specific humoral immune responses. Blood *109*, 212–218.

Yoshida, N., Ikeda, Y., Notomi, S., Ishikawa, K., Murakami, Y., Hisatomi, T., Enaida, H., and Ishibashi, T. (2013a). Laboratory evidence of sustained chronic inflammatory reaction in retinitis pigmentosa. Ophthalmology *120*, e5–e12.

Yoshida, N., Ikeda, Y., Notomi, S., Ishikawa, K., Murakami, Y., Hisatomi, T., Enaida, H., and Ishibashi, T. (2013b). Clinical evidence of sustained chronic inflammatory reaction in retinitis pigmentosa. Ophthalmology *120*, 100–105.

Zabel, M.K., Zhao, L., Zhang, Y., Gonzalez, S.R., Ma, W., Wang, X., Fariss, R.N., and Wong, W.T. (2016). Microglial phagocytosis and activation underlying photoreceptor degeneration is regulated by CX3CL1-CX3CR1 signaling in a mouse model of retinitis pigmentosa. Glia *64*, 1479–1491.

Zeng, H.Y., Zhu, X.A., Zhang, C., Yang, L.P., Wu, L.M., and Tso, M.O. (2005). Identification of sequential events and factors associated with microglial activation, migration, and cytotoxicity in retinal degeneration in rd mice. Invest. Ophthalmol. Vis. Sci. *46*, 2992–2999.

Zhao, L., Zabel, M.K., Wang, X., Ma, W., Shah, P., Fariss, R.N., Qian, H., Parkhurst, C.N., Gan, W., and Wong, W.T. (2015). Microglial phagocytosis of living photoreceptors contributes to inherited retinal degeneration. EMBO Mol. Med. *7*, 1179–1197.

Zhong, X., Gutierrez, C., Xue, T., Hampton, C., Vergara, M.N., Cao, L.H., Peters, A., Park, T.S., Zambidis, E.T., Meyer, J.S., et al. (2014). Generation of three-dimensional retinal tissue with functional photoreceptors from human iPSCs. Nat. Commun. *5*, 4047.

Zhu, J., Cifuentes, H., Reynolds, J., and Lamba, D.A. (2017). Immunosuppression via loss of IL2rγ enhances long-term functional integration of hESC-derived photoreceptors in the mouse retina. Cell Stem Cell *20*, 374–384.e5.